https://doi.org/10.1016/j.actamat.2018.09.014

Nanocrystalline Ag-W alloys lose stability upon solute desegregation from grain boundaries

Z. B. Jiao[1,2], C. A. Schuh[1,*]

[1] Department of Materials Science and Engineering, Massachusetts Institute of Technology, 77 Massachusetts Avenue, Cambridge, MA 02139, USA

[2] Department of Mechanical Engineering, The Hong Kong Polytechnic University, Hung Hom, Kowloon, Hong Kong, China

Abstract

Alloying has proven an enabling strategy to stabilize nanocrystalline materials against grain growth, especially in cases where the solute segregates to grain boundaries and lowers their energy. Among such materials reported to date, most all are stable up to some temperature at which second phases precipitate, depleting solute from the boundaries. Here in contrast we present a system that loses stability by thermal desegregation of solute back into solution in the grains. Specifically, we explore minor additions of W (0, 0.3, 1.3, and 1.9 at.%) on the grain structure, grain boundary segregation, and thermal stability of nanocrystalline Ag using transmission electron microscopy and atom probe tomography. W is shown to segregate at grain boundaries in electrodeposited nanocrystalline Ag, pushing the onset temperature for grain growth from ~ 200 °C up to ~300 ºC. Upon such heating we observe the dissolution of W off the grain boundaries and back into the FCC host lattice, at a temperature in line with thermodynamic expectations on the basis of the segregation isotherm.

Keywords: Nanocrystalline alloys, Ag-W alloys, grain boundary segregation, stability

1. Introduction

The addition of alloying elements can stabilize the grain structure of nanocrystalline alloys, either through kinetic constraints on coarsening or through thermodynamic reduction of the driving forces for coarsening, or both [1-8]. For instance, ball-milled W-Ti alloys have been shown to have nanocrystalline grain structures that do not coarsen appreciably even after heating to temperatures up to ~1100 °C [9], while Fe-Zr and Fe-Cr-Hf nanocrystalline alloys exhibit stability to temperatures as high as 900 °C [10,11]. In these nanocrystalline alloys, the minority solute additions are added for their tendency to segregate to grain boundaries, where they lower the grain boundary energy and bring the system closer to thermodynamic equilibrium, thereby dramatically enhancing nanocrystalline stability.

Grain boundary segregation, however, is just one possible configurational option for solutes added to a nanocrystalline alloy, and in all of these systems the energetic competition between the grain-boundary segregated state and other configurations—such as solvation or second phase precipitation—is typically very close. If the temperature is high enough, solute-stabilized nanocrystalline alloys undergo instabilities as other alloy configurations become favorable, which result in grain coarsening. In Fig. 1 we illustrate a few instability mechanisms by which grain boundaries can become 'unlocked' from solute segregation.

The most commonly observed cause of nanocrystalline instability is the loss of grain boundary segregation by the formation of second phases at elevated temperatures (scheme I in Fig. 1). The second phase can be an intermetallic compound (if the alloy system has a negative enthalpy of mixing, such as in Co-P [12], Pd-Zr [13], Y-Fe [14]) or an elemental precipitate (if the alloy system has a positive enthalpy of mixing like Fe-Ag [15] or Cu–Nb [16]). Upon the formation of

second phases, solute segregation at grain boundaries is typically reduced, increasing the driving force for grain growth. Table 1 lists a number of studies in which precipitation is associated with the loss of nanocrystalline stability [9-29].

Interestingly, most of the above studies have focused on highly-alloyed nanocrystalline alloys. However, a few studies have found that stable nanocrystalline structures can also be achieved in more dilute alloys with 2 at.% or less solute [23,25]. Dilute systems are scientifically interesting, especially in cases where the total alloying addition is near or below the solid solubility limit of the bulk metal. Such systems are more likely to exhibit instability by the other schemes in Fig. 1. For example, if grain boundary segregation is weak, i.e., insufficient to saturate the boundaries and offset their intrinsic defect energy, grain boundaries can migrate away from the solutes, forcing them into solution (scheme II in Fig. 1). An example is the Fe-Cu system (see also Table 1); Eckert et al. reported that ball-milled nanocrystalline Fe initially had Cu segregation at grain boundaries that was too weak to effectively suppress the grain boundary migration and thus grain growth ensued at elevated temperatures [30]. Interestingly, this is also viewed as a metastable condition, as eventually the dissolved Cu atoms accumulate and transform to Cu precipitates, which further promotes instability via scheme I.

A third scheme of instability that involves solute dissolution off of grain boundaries is schematized in scheme III of Fig. 1. Thermal desegregation of solute is the expected instability in stable nanocrystalline alloys in an equilibrium condition at low temperatures [31]. Upon heating they are expected to gradually lose solute into solution and the grain size increase accordingly, in what is effectively a second-order phase transition between a solute-segregated nanocrystalline condition and a solutionized bulk coarse-grained alloy at high temperatures. However, at the time of this writing we are not aware of any experimental observation of this mode of instability.

Like scheme II described above, scheme III is perhaps more likely to be observed in a dilute nanocrystalline alloy. In addition to their scientific interest, dilute nanocrystalline alloys are also technologically attractive, as they may achieve stable nanocrystalline grains with the attendant improved mechanical properties, without as significantly compromising other physical properties, such as electrical conductivity, which might be adversely affected by heavy alloying. For example, nanocrystalline Ag has long been considered a promising material for electronic applications because of its high electrical conductivity and high hardness/strength in nanocrystalline form, but what nanocrystalline variants of silver have been evaluated [32-36] end up exhibiting insufficient structural stability. Alloying nanocrystalline Ag with a second element that is specifically chosen for its ability to decorate grain boundaries and stabilize a nanoscale grain size is therefore of interest. In particular, dilute nanocrystalline Ag alloys with minor alloying additions are highly desirable in order to achieve a good combination of thermal, mechanical and electrical properties.

In this work we investigate the influence of dilute W additions (0, 0.3, 1.3, and 1.9 at.%) on the grain structure, elemental distribution, and grain boundary segregation of electrodeposited nanocrystalline Ag alloys at different annealing temperatures, and further to correlate the grain structure and chemical distribution with the stability of these dilute nanocrystalline alloys. We show that this system exhibits instability by grain boundary desegregation into solution, i.e., scheme III in Fig. 1, the first such system of which we are aware.

2. Experimental

Four Ag-W alloy foils were acquired from Xtalic Corporation (Marlborough, MA), under the trade name LUNA, having been prepared through a process of complexed aqueous electrodeposition that permits the induced co-deposition of W and Ag despite their very different

reduction potentials [37]. Each film was about 2 μm in thickness, and was provided with an area of about 2 cm^2. The deposit compositions were measured using a JEOL-JXA-8200 electron probe micro-analyzer (EPMA) in the wavelength dispersive mode, and the average composition from ten different measurements for each sample is reported in Table 2. For convenience, the four alloys are hereafter referred to as the 0W, 0.3W, 1.3W, and 1.9W alloys. Small samples of the as-deposited alloys were sealed in a quartz tube under a vacuum of 10^{-3} Torr and then isothermally annealed for 24 h at temperatures in the range 100-400 °C in a box furnace.

Transmission electron microscopy (TEM) specimens were prepared using the lift-out method in an FEI Helios focused ion beam (FIB). The FIB lamellae were cut perpendicular to the alloy film surface and positioned on a Cu grid. Final thinning was performed at 2 keV to minimize damage. TEM and selected area electron diffraction (SAED) measurements were conducted on a JEOL 2010 FEG microscope operated at 200 keV. For each sample, grains were manually identified and traced using a combination of dark-field and bright-field imaging, and the equivalent circular diameter was calculated.

Needle-shaped specimens required for atom probe tomography (APT) were fabricated by FIB lift-out and annular milling in an FEI Helios. The first stages of milling were performed with a 30 keV Ga+ ion beam and a current of 0.1-1 nA, and the final polishing was performed at 2 keV Ga+ and 10-30 pA either in annular milling or broad beam mode. APT characterizations were performed in a CAMECA Instruments LEAP 4000X HR local electrode atom probe. The APT specimens were analyzed in laser mode with a specimen temperature of ~30 K, a focused laser beam energy of 30 pJ, a pulse repetition rate of 100 kHz, a pulse fraction of 0.2, and an ion collection rate of 0.5% ions per field evaporation pulse. Imago Visualization and Analysis Software (IVAS) version 3.6.12 was used for creating the 3D reconstructions and data analysis.

Autocorrelation functions of composition fluctuations in the Ag-W alloys were calculated using a custom-written MATLAB (Mathworks Inc.) script.

3. Results

3.1 Grain structure in the as-deposited state

Representative TEM micrographs showing the cross-sectional grain structures of the as-deposited 0W, 0.3W, 1.3W, and 1.9W alloys in both bright- and dark-field modes, together with the associated SAED patterns, are presented in Fig. 2, with average grain sizes listed in Table 2. The as-deposited samples all have a uniform and apparently equiaxed nanocrystalline structure, and the SAED pattern confirms a fine-grained fcc structure with no evidence for additional phases. The 0W alloy exhibits an equiaxed grain structure with an average grain size of approximately 27 ± 10 nm in the as-deposited state (Fig. 2a). The addition of a minor W addition (Fig. 2b-d) has no strong effect on the as-deposited grain structure, with the average grain sizes of the alloy samples all lying in the range of 20-30 nm.

3.2 Chemical distribution in the as-deposited state

Representative APT atom maps clipped from a larger dataset are shown in Fig. 3a-d for the 0W, 0.3W, 1.3W, and 1.9 W alloys, respectively, in which Ag and W atoms are depicted by blue and red dots, respectively. The Ag distribution of the 0W alloy is shown in Fig. 3a (only 0.5% of atoms are shown for clarity), and the Ag atom maps of other alloys show very similar results and are thus not shown; the distribution of Ag atoms appears fairly uniform, and no grain structure can be readily observed from the Ag atom maps alone. In contrast, the distributions of W atoms are quite non-uniform, and W-enriched and W-depleted regions are clearly distinguishable in the 0.3W,

1.3W, and 1.9W alloys (Fig. 3b-d). Moreover, the segregation pattern of the W-enriched region exhibits a network-like structure that is suggestive of grains, with a length-scale of approximately 20-30 nm, matching the grain size in these as-deposited samples (cf. Fig. 2).

To further understand the grain structure in these APT data, the distributions of Ga atoms are also included in Fig. 3, depicted as grey dots, which originate from implantation during the FIB-based APT specimen preparation. The overall level of Ga implantation is low in all the APT tips, less than 1 at.%; this level of damage is unlikely to have significantly affected the grain structures of these nanocrystalline alloys. It has previously been documented that Ga ions prefer to penetrate through grain boundaries of many nanocrystalline materials, and ultimately remain incorporated into these grain boundaries after FIB milling [38-40]. Therefore, the distribution of Ga atoms can serve to mark grain boundaries in the APT reconstructions. In the as-deposited state, the distribution of Ga atoms exhibits a grain-structure-like network, which in every case is quite similar to the distribution of W. The co-location of W and Ga becomes more obvious by combining the Ga and W atom maps together, as illustrated in the rightmost column of Fig. 3b-d. This result provides a strong indication that W atoms are preferentially segregated along the grain boundaries of the nanocrystalline Ag-W alloys in the as-deposited state.

A measurement of the mean wavelength of the composition fluctuations in Fig. 3 can be obtained through use of the autocorrelation function [41], as used in previous APT studies to measure the size of nanocrystalline grains decorated with solutes [42]. Plots of the autocorrelation function, R_k, averaged over 100 randomly chosen center points with a *k*-resolution of 0.3 nm, are shown in Fig. 4a-c for the 0.3W, 1.3W, and 1.9W alloys, respectively. The characteristic length scale of the W distribution is indicated by the first non-trivial maximum in R_k, as marked with arrows, and is found to be 22, 20, and 21 nm for the 0.3W, 1.3W, and 1.9W alloys, respectively.

These values are in good agreement with the TEM measured grain sizes of the Ag-W alloys (d = 24 ± 8, 24 ± 9, and 23 ± 8 nm, respectively), again providing evidence for W segregation at grain boundaries in these as-deposited nanocrystalline Ag alloys.

Quantitative compositional analysis of W grain boundary segregation was conducted using 1D concentration profiles. Representative profiles of W and Ga are displayed in Fig. 5a-c, taken across two Ga-enriched boundaries in the 0.3W, 1.3W, and 1.9W alloys, respectively. The concentration peaks of W and Ga align and are taken to denote the location of grain boundaries. For each specimen, the W content at grain boundaries (X_{gb}) and in the grain interior (X_{gi}) were measured by averaging over 10 such scans. The W content in grain interior regions in the 0.3W, 1.3W, and 1.9W alloys are measured to be 0.25 ± 0.08, 0.48 ± 0.06, 0.63 ± 0.09 at.%, respectively, while the respective contents at the grain boundaries are estimated to be 2.4 ± 0.9, 2.8 ± 1.2, and 3.0 ± 1.4 at.%. However, we note that the width of the W segregation zone is usually over-represented in APT data, due to local magnification effects associated with trajectory aberrations caused by atoms sitting near grain boundaries. As a result, the segregated solute at grain boundaries is spread more broadly in the APT data than it is in the true specimen, and the true grain boundary composition levels are higher than those observed. One way to correct for such blurring of the signal is to integrate the composition profiles from the APT data across the boundary, and assign the excess W concentration uniformly to a grain boundary of finite thickness, t. Performing this correction on the above values for a thickness t = 1 nm gives respective compositions of 15.1 ± 2.1, 10.7 ± 1.4, 14.1 ± 1.5 at.%, for example.

3.3 Grain structure in the annealed state

To investigate the effect of W additions on the thermal stability of nanocrystalline Ag alloys, we selected three compositions to focus on, namely 0W, 0.3W, and 1.3W alloys, pieces of which were annealed for 24 h at 100, 200, 300, and 400 °C in vacuum. Representative bright-field TEM images and inset SAED patterns of the annealed alloys are shown in Fig. 6, and their average grain sizes are plotted in Fig. 7 as a function of annealing temperature. At 100 °C, the grain structures look about the same as they do in the as-deposited condition (cf. Fig. 2), indicating that little or no grain growth occurs in this condition. After annealing for 24 h at 200 °C, grain growth can be observed in the 0W alloy, with the average grain size growing from 27 ± 10 nm to 38 ± 13 nm, whereas the 0.3W and 1.3W alloys do not exhibit significant changes in grain size, remaining below 30 nm.

With the annealing temperature further increasing to 300 °C, the 0W alloy shows an obvious increase in grain size (65 ± 27 nm), which is more than double that in the as-deposited state (27 ± 10 nm). The 0.3W and 1.3W alloys also begin to exhibit grain growth at 300 °C, to grain sizes of 54 ± 26 and 43 ± 16 nm, respectively, still smaller than that of the 0W alloy in the same condition. Annealing at 400 °C results in dramatic grain growth in all three alloys, with grain sizes crossing above the threshold of 100 nm that defines a nanocrystalline material, and reaching sizes of several hundreds of nanometers. The inset SAED patterns in Fig. 6 are also consistent with grain coarsening, where the diffraction lines become discontinuous and eventually form discrete spots as fewer grains are sampled.

3.4 Chemical distribution in the annealed state

The 1.3W alloy, being the most stable of those alloys in Fig. 7, was selected as a representative to study the evolution of grain boundary segregation with annealing temperature.

The distributions of Ga and W atoms are shown in Fig. 8, while representative Ga and W profiles across Ga-enriched boundaries are presented in Fig. 9a-d for the 100, 200, 300, and 400 °C annealed samples, respectively. At 100 °C (Fig. 8a), the 1.3W alloy exhibits a similar elemental distribution of W and Ga as observed in the as-deposited specimen; Ga atoms still show a network-like pattern highlighting the grain boundaries, and W atoms are clearly segregated to those grain boundaries. The average W peak concentration was estimated to be ~14.5 ± 2.8 at.% after correcting to a grain boundary thickness of t = 1 nm (Fig. 9a), similar to that in the as-deposited sample above (10.7 ± 1.4 at.%). The same basic conclusion can be drawn from the sample annealed at 200 °C; this structure is essentially the one that was deposited in the first place, with W segregated on the grain boundaries (Figs. 8b, 9b).

Recall that at 300º C we observed the first signs of grain growth in this alloy (Figs. 6 and 7), and at this temperature we also begin to see changes in the W distribution as well. In Fig. 8c the Ga atoms still highlight a grain boundary network, but the distribution of W atoms appears considerably more homogeneous than it did at the lower annealing temperatures. The distributions of W and Ga atoms are less visually correlated in these atom maps, implying a weakening of W grain boundary segregation, after annealing for 24 h at 300 °C. From the concentration profile in Fig. 9c, we see that there is still W enrichment at the boundaries, although it is a weaker signal than we have previously seen. The grain boundary W content is estimated to be 7.1 ± 1.5 at.% after correcting to a grain boundary thickness of t = 1 nm, lower than the 10.7 ± 1.4 at.% seen in the as-deposited condition.

This trend of thermal desegregation of W from grain boundaries continues to its logical conclusion in Fig. 8d at 400º C. With a very large grain size of several hundred nanometers, the APT samples far fewer grain boundaries, as reflected in the Ga distribution. What is more, the W

atoms are homogeneously distributed throughout the whole volume of analysis, and no W enrichment at grain boundaries can be observed. The absence of W segregation at grain boundaries can also be quantitatively verified by the W concentration profile in Fig. 9d.

4. Discussion

The above results show that W additions play a role in enhancing the stability of nanocrystalline Ag alloys at 200 °C. At this temperature grain growth already begins to occur in the unalloyed Ag specimen, but no sort of structural change is seen in the alloyed specimens, which all exhibit W segregation at the grain boundaries before and after annealing. However, the gradual de-segregation of W off grain boundaries was observed starting from 300 °C, and, along with it, the onset of grain growth. In the following sections, we discuss in more detail the grain boundary segregation and its correlation with the stability of the nanocrystalline Ag alloys.

4.1 Grain boundary segregation and stability

The co-location of W and Ga, together with direct correspondence between the length-scales of the APT composition fluctuations and TEM grain sizes, strongly supports that W atoms are preferentially segregated at the grain boundaries of these nanocrystalline Ag alloys. The improved stability of the Ag-W alloys after annealing for 24 h at 200 °C is quite likely related to this grain boundary segregation, which would involve kinetic drag effects as well as a primary thermodynamic effect of lowering the grain boundary energy. Grain boundary segregation may be driven by a number of factors, including mismatches in chemical, interfacial and elastic energies. Murdoch and Schuh [44] developed a modified Miedema model to estimate the dilute-limit grain

boundary segregation enthalpy, i.e., independent of temperature and grain boundary solute concentration, as given by:

$$\Delta H^{seg} = -0.71 \times \frac{1}{3} \times v \times (-\Delta H^{\text{int}}_{W \text{ in } Ag} - c_0 \gamma^S_{Ag} V^{2/3}_{Ag} + c_0 \gamma^S_W V^{2/3}_{Wg}) + \Delta E_{el} \quad (1)$$

where v = 0.5 is a geometrical parameter describing the fraction of bulk bonds lost by an atom at the grain boundary, and $\Delta H^{\text{int}}_{W \text{ in } Ag}$ is the bulk interaction energy (i.e., the bond-level heat of mixing) of W atoms in Ag. The interfacial energies are captured in the difference between the values of $c_0 \gamma^S_{Ag} V^{2/3}_{Ag}$ and $c_0 \gamma^S_W V^{2/3}_W$, where c_0 is a semi-empirical constant, taken as 4.5×10^8 [44], γ^S is the surface energy and V is the atomic volume of the atomic species denoted by the subscript (each of these properties should be reflective of the pure components in the same notional FCC lattice). ΔE_{el} is the elastic strain energy associated with solute atomic size misfit, which can be calculated as [44]:

$$\Delta E_{el} = \frac{24 K_{Ag} G_W r_{Ag} r_W (r_W - r_{Ag})^2}{3 K_{Ag} r_{Ag} + 4 G_W r_W} \quad (2)$$

where K is the bulk modulus, G is the shear modulus, and r is the atomic radius of the species denoted by the subscript, in the FCC lattice.

With input values of $\Delta H^{\text{int}}_{W \text{ in } Ag}$ = 172 kJ mol^{-1} [45], γ^S_{Ag} = 1.25 J m^{-2} [46], γ^S_W = 2.68~3.11 J m^{-2} [47], V_{Ag} = 10.28 cm^3 mol^{-1} [48], V_W = 6.13 cm^3 mol^{-1} [49], r_{Ag} = 0.144 nm [48], r_W = 0.137 nm [48], K_{Ag}= 100 GPa [45], and G_W = 157 GPa [49], the grain boundary segregation enthalpy for W in Ag is calculated to be in the range of 1.7~9.4 kJ mol^{-1}. Such values are moderate and comparable to those of some other thermodynamically stabilized nanocrystalline alloys studied in the literature, such as Ni-W (~9 kJ mol^{-1}), Cu-Au (~10 kJ mol^{-1}) and Ni-Cu (~12 kJ mol^{-1}) [44].

Importantly, such a positive grain boundary segregation enthalpy does suggest that W segregation in Ag-W should lower the grain boundary formation energy, providing some degree of thermodynamic stability to the nanocrystalline structure.

Having estimated the grain-boundary segregation enthalpy in the Ag-W system, we can now calculate the theoretical level of grain-boundary segregation of W expected in equilibrium. A simple isotherm that has been used extensively to estimate the segregation enthalpy is that of McLean, given by [50]:

$$\frac{X_{gb}}{1-X_{gb}} = \frac{X_{gi}}{1-X_{gi}} \exp\left(\frac{\Delta H_{seg}}{RT}\right) \quad (3)$$

where X_{gb} and X_{gi} are the composition of the grain boundary and grain interior, respectively; R is the gas constant and T is temperature. We use Eq. (3) to calculate the equilibrium values of W concentration at grain boundaries, X_{gb}, in the Ag-W alloys, by taking the range of grain-boundary segregation enthalpies, ΔH^{seg}, from the Miedema model above (1.7~9.4 kJ mol^{-1}), the grain interior composition, X_{gi}, from the APT measurements, and the grain size, d, from the TEM measurements.

The resulting predicted range of the X_{gb} values in the 0.3W, 1.3W and 1.9W alloys in the as-deposited condition, as well as the 1.3W alloy in the 100 and 200 °C annealed conditions, are summarized in Fig. 10. For comparison, the experimental values of grain boundary segregation obtained from APT (after grain boundary thickness correction) are also included in Fig. 10. It is important to note that this analysis is quite approximate in several senses. In addition to the simplicity of the analytical segregation model above, the uncertainty of which is reflected in the bars on Fig. 10, the experimental measurements of grain boundary segregation are also subject to uncertainty based on the thickness correction we have used. To reflect the possible range of

variability in the experimental values we include broad error bars in Fig. 10, showing the range of compositions that can emerge if the grain boundary thickness is assigned more extreme values of t = 0.5 or 1.5 nm (as compared to the default 1 nm that we have used). Nonetheless, in spite of these issues, it is encouraging to see that most of the APT measured values are reasonably close to the equilibrium segregation predictions, within the uncertainty of this very approximate analysis.

It is interesting to find that the as-electrodeposited samples exhibit near-equilibrium grain boundary segregation levels based on this analysis. This could be considered nominally surprising in light of the nonequilibrium nature of electrodeposition. However, similar near-equilibrium segregation of solute elements at grain boundaries in electrodeposited samples have also been observed in other nanocrystalline alloy systems, such as Ni-P [27], Ni-W [28], and Al-Mn [39,51]. In those studies, one possible interpretation has been put forward that the electrodeposition process may be sufficiently close to equilibrium growth that the system is able to find near-equilibrium conditions and grow grain structures with preferred grain-boundary segregation states. For example, Ruan and Schuh [51] estimated the surface diffusion distance of atoms on the surface of an Al-Mn film. They calculated that in the time required to deposit one monolayer, the surface atom diffusion distance is approximately 18 nm. In Ref. [39] it was argued that this distance, being of the order of the grain size, supports significant solute redistribution during deposition, with solutes being able to find exposed grain boundary sites before being buried by subsequent deposition. A similar argument may apply in the present case; considering the similar surface diffusivities of Al (~3.7×10^{-11} cm^{-2} s^{-1}) and Ag (~1.0×10^{-11} cm^{-2} s^{-1}) [52] at ambient temperatures, a diffusion distance on the order of tens of nanometers is reasonable for the nanocrystalline Ag alloys, which is of the same order of magnitude as the grain size of our Ag-W alloys (20~40 nm). Surface diffusion is also expected to be accelerated in electrochemical conditions. In this scenario,

most atoms are likely to experience both grain interior and grain-boundary regions as they diffuse along the surface during electrodeposition and might assemble into a near-equilibrium segregation state.

4.2 Grain-boundary de-segregation and instability

As noted in the introduction and laid out in Table I, we find that most all nanocrystalline alloys studied in detail in the literature undergo instability through some kind of phase separation upon heating, after which grain growth is a trailing consequence. Therefore, the most striking result in the present work is that loss of stability in our Ag-W alloys appears to be associated with grain boundary desegregation by dissolution of W into the bulk. Grain growth of the 1.3W alloy begins to be observed after 24 hours at 300 °C, and is accompanied by a measurable reduction of W segregation at grain boundaries (Figs. 9a-c). Meanwhile, there is a concomitant increase in W concentration in the grain interior region, from 0.53 at.% at 200 °C to 0.67 at.% at 300 °C and further to 0.70 at.% at 400 °C, moving closer to the global W concentration.

This dissolution is also not associated with any observation of a competing second phase. Considering that the volume of a single APT tip (~50 × 50 × 300 nm) is equivalent to a volume of more than 20 grains (grain size of 38 ± 13 nm at 300 °C), the precipitation of second phases at grain boundaries, if any, should be detectable by APT. For each condition we examined at least two APT tips, but observed no W-enriched clusters at all. We also searched for possible second phases in the 300 and 400 °C samples using TEM and SAED, but no evidence for formation of second phases can be observed in these data either (neither at grain boundaries nor within grain interiors). Therefore, by combining the APT and TEM measurements, the possibility that the

nanocrystalline instability arises from the precipitation of second phases (Scheme I in Fig. 1) can be reasonably ruled out.

A second, previously documented mode of instability that does not require second phase precipitation is that of Scheme II in Fig. 1, which pertains to grain-boundary migration away from the solutes. If this mechanism of instability were present in our Ag-W specimens, then we would expect that the network-like structure of W segregation, observed at low temperatures (Figs. 8a and b), would be retained at the prior grain boundaries after having been detached from them by migration/grain growth. However, the distribution of W remains explicitly at the grain boundaries in the 300 °C condition (Fig. 8c and 9c), associated with the Ga fiducial markings there; there is no evidence of detachment of the boundaries from W. In the 400 °C condition, all of the W atoms are distributed uniformly across the volume of analysis, and no network-like structure can be observed. These observations suggest that W is clearly mobile and not stuck in a network at the prior grain boundaries at these temperatures. Therefore, we also rule out the possibility that Ag-W loses its nanocrystalline stability due to the grain-boundary migration away from solute (Scheme II in Fig. 1).

Having ruled out the two previously-documented mechanisms of instability (Schemes I and II in Fig. 1) for nanocrystalline Ag-W, we suggest instead that the present work constitutes a demonstration of Scheme III: the direct dissolution of solutes off of the grain boundaries and into the bulk FCC phase. The McLean isotherm (Eq. (3)) provides a simple basis for the description of the temperature dependence of grain-boundary segregation, as desegregation completes at the temperature where when the grain boundary composition, X_{gb}, equals the grain interior composition, X_{gi}. Therefore, the temperature at which the grain boundary would desegregate entropically is:

$$T \approx \frac{\Delta H_{seg}}{R} \tag{4}$$

From Section 4.1, the grain-boundary segregation enthalpy, ΔH_{seg}, calculated from the modified Miedema model is in the range of 1.7~9.4 kJ mol^{-1}. Using a median value of 5.5 kJ mol^{-1}, the critical temperature for grain-boundary desegregation is estimated to be around 380 °C. This value agrees well with our experimental observation that the grain-boundary segregation starts to decrease at 300 °C and there is no grain boundary segregation at 400 °C (cf. Fig. 9). In this scenario, the entropic desegregation off the grain boundaries would lead to an increased rate of coarsening and a loss of stability against grain growth upon annealing, exactly as observed in Fig. 6.

One possible concern with this interpretation is that the dissolution of W into the bulk at 400 ºC that we see in these experiments suggest a solid solubility of at least 1.3 at% W in Ag at this temperature. This value is beyond that predicted by the version of the Ag-W phase diagram in Ref. [53], which suggests very low mutual solubility in the solid state at any temperature. However, this phase diagram is based on very limited experimental data and may need some modification. Additionally, it is plausible that the presence of W would stabilize lattice vacancies in Ag [54,55], lowering vacancy formation energies and enhancing the solubility of W. Interestingly, such an effect might also facilitate bulk diffusion of W in Ag, which is certainly needed for dissolution off of the grain boundaries following Scheme III. The paucity of both thermodynamic and kinetic data for this alloy system beg for future studies to resolve such issues.

5. Summary

Based on an experimental study of the effect of dilute additions of W on the grain structure, grain-boundary segregation, and thermal stability of nanocrystalline Ag-W alloys, the following conclusions are drawn:

1. In the as-deposited condition, the 0W, 0.3W, 1.3W, and 1.9W alloys all exhibit an equiaxed grain structure with an average grain size of 20~30 nm. APT reveals that W exhibits segregation at grain boundaries, as seen directly when compared against Ga fiducials that mark the grain boundaries, and indirectly through an autocorrelation analysis of the W distribution. Using a Miedema model, the enthalpy of grain boundary segregation is estimated to be in the range of 1.7~9.4 kJ mol^{-1} for W in Ag, which corresponds to grain boundary enrichments in reasonable agreement with our experiments in the as-deposited condition.
2. Whereas pure nanocrystalline Ag exhibits obvious grain growth after annealing for 24 h at 200 °C, Ag-W alloys with grain boundary segregation show enhanced stability with no structural changes under the same condition. The enhanced stability of nanocrystalline Ag-W alloys can be attributed to the segregation.
3. Most interestingly, as the temperature further increases, we observe a gradual loss of grain boundary segregation, by direct entropic dissolution into solution in the silver host lattice. This transition begins at 300 ºC with a reduction in grain boundary segregation, and is complete by 400 °C where the grain size runs away into the microcrystalline regime.
4. Our analysis thus presents what may be the first experimental demonstration of Scheme III in Fig. 1, namely, an alloy in which the loss of nanocrystalline stability is effected by grain boundary desegregation into the bulk, without second phase formation. Interestingly, this is the mechanism of stability loss expected in fully enthalpically stable nanocrystalline

alloys, and corresponds to a second-order phase transition between a stable nanocrystalline state and a stable bulk solution.

Acknowledgement

This research was supported by the U.S. Army Research Office under grant W911NF-14-1-0539 and the U.S. National Science Foundation under grant DMR 1606914. ZBJ would like to acknowledge the support from The Hong Kong Polytechnic University (1-ZE8D). The authors thank A. Kalidindi of MIT for valuable discussions.

References

[1] J. Weissmüller, Alloy effects in nanostructures, Nanostruct. Mater. 3 (1993) 261-272.

[2] R. Kirchheim, Grain coarsening inhibited by solute segregation, Acta Mater. 50 (2002) 413-419.

[3] F. Liu, R. Kirchheim, Grain boundary saturation and grain growth, Scr. Mater. 51 (2004) 521-525.

[4] P.C. Millett, R.P. Selvam, A. Saxena, Stabilizing nanocrystalline materials with dopants, Acta Mater. 55 (2007) 2329-2336.

[5] J.R. Trelewicz, C.A. Schuh, Grain boundary segregation and thermodynamically stable binary nanocrystalline alloys, Phys. Rev. B 79 (2009) 094112.

[6] H.A. Murdoch, C.A. Schuh, Stability of binary nanocrystalline alloys against grain growth and phase separation, Acta Mater. 61 (2013) 2121-2132.

[7] D.L. Beke, C. Cserhati, I.A. Szabo, Segregation inhibited grain coarsening in nanocrystalline alloys, J. Appl. Phys. 95 (2004) 4996-5001.

[8] C.C. Koch, R.O. Scattergood, K.A. Darling, J.E. Semones, Stabilization of nanocrystalline grain sizes by solute additions. J. Mater. Sci. 43 (2008) 7264-7272.

[9] T. Chookajorn, H.A. Murdoch, C.A. Schuh, Design of stable nanocrystalline alloys, Science 337 (2012) 951-954.

[10] K.A. Darling, B.K. VanLeeuwen, C.C. Koch, R.O. Scattergood, Thermal stability of nanocrystalline Fe–Zr alloys, Mater. Sci. Eng. A 527 (2010) 3572-3580.

[11] W. Xu, L. Li, M. Saber, C.C. Koch, Y. Zhu, R.O. Scattergood, Microstructures and stabilization mechanisms of nanocrystalline iron-chromium alloys with hafnium addition, Metall. Mater. Trans. A 46 (2015) 4394-4404.

[12] P. Choi, M. da Silva, U. Klement, T. Al-Kassab, R. Kirchheim, Thermal stability of electrodeposited nanocrystalline Co-1.1 at.% P, Acta Mater. 53 (2005) 4473-4481.

[13] B.K. VanLeeuwen, K.A. Darling, C.C. Koch, R.O. Scattergood, B.G. Butler, Thermal stability of nanocrystalline $Pd_{81}Zr_{19}$, Acta Mater. 58 (2010) 4292-4297.

[14] J. Weissmuller, W. Krauss, T. Haubold, R. Birringer, H. Gleiter, Atomic structure and thermal stability of nanostructured Y-Fe alloys, Nanostruct. Mater. 1 (1992) 439.

[15] F. Liu, Grain growth in nanocrystalline Fe–Ag thin film, Mater. Lett. 59 (2005) 1458-1462.

[16] M. Saber, H. Kotan, C.C. Koch, R.O. Scattergood, Thermodynamic stabilization of nanocrystalline binary alloys, J. Appl. Phys. 113 (2013) 063515.

[17] K. Santhi, E. Thirumal, S.N. Karthick, H.J. Kim, M. Nidhin, V. Narayanan, A. Stephen, Synthesis, structure stability and magnetic properties of nanocrystalline Ag–Ni alloy, J. Nanopart. Res. 14 (2012) 868.

[18] Y. Purohit, S. Jang, D.L. Irving, C.W. Padgett, R.O. Scattergood, D.W. Brenner, Atomistic modeling of the segregation of lead impurities to a grain boundary in an aluminum bicrystalline solid, Mater. Sci. Eng. A 493 (2008) 97-100.

[19] T.Y. Huang, A.R. Kalidindi, C.A. Schuh, Grain growth and second-phase precipitation in nanocrystalline aluminum–manganese electrodeposits, J. Mater. Sci. 53 (2018) 3709-3719.

[20] T. Spassov, L. Lyubenova, Y. Liu, S. Bliznakov, M. Spassova, N. Dimitrov, Mechanochemical synthesis, thermal stability and selective electrochemical dissolution of Cu–Ag solid solutions, J. Alloy. Compd. 478 (2009) 232-236.

[21] X. Chen, J. Mao, Thermal stability and tensile properties of electrodeposited Cu-Bi alloy, J. Mater. Eng. Perf. 20 (2011) 481-486.

[22] G. Csiszár, S.J.B. Kurz, E.J. Mittemeijer, Stability of nanosized alloy thin films: Faulting and phase separation in metastable Ni/Cu/Ag-W films, Acta Mater. 110 (2016) 324-340.

[23] M.A. Atwater, R.O. Scattergood, C.C. Koch, The stabilization of nanocrystalline copper by zirconium, Mater. Sci. Eng. A 559 (2013) 250-256.

[24] Y.Z. Chen, A. Herz, Y.J. Li, C. Borchers, P. Choi, D. Raabe, R. Kirchheim, Nanocrystalline Fe–C alloys produced by ball milling of iron and graphite, Acta Mater. 61 (2013) 3172-3185.

[25] K.A. Darling, B.K. VanLeeuwen, J.E. Semones, C.C., Koch, R.O. Scattergood, L.J. Kecskes, S.N. Mathaudhu, Stabilized nanocrystalline iron-based alloys: guiding efforts in alloy selection, Mater. Sci. Eng. A 528 (2011) 4365-4371.

[26] E. Pellicer, A. Varea, K.M. Sivaraman, S. Pané, S. Surinach, M.D. Baró, J. Nogués, B.J. Nelson, J. Sort, Grain boundary segregation and interdiffusion effects in nickel–copper alloys: an effective means to improve the thermal stability of nanocrystalline nickel, ACS Appl. Mater. Inter. 3 (2011) 2265-2274.

[27] B. Färber, E. Cadel, A. Menand, G. Schmitz, R. Kirchheim, Phosphorus segregation in nanocrystalline Ni–3.6 at.% P alloy investigated with the tomographic atom probe (TAP), Acta Mater. 48 (2000) 789-796.

[28] A.J. Detor, C.A. Schuh, Grain boundary segregation, chemical ordering and stability of nanocrystalline alloys: Atomistic computer simulations in the Ni–W system, Acta Mater. 55 (2007) 4221-4232.

[29] Y.R. Abe, W.L. Johnson, Stability of nanocrystalline structures in the Ti-Cu system, Mater. Sci. Forum 88 (1992) 513-520.

[30] J. Eckert, J.C. Holzer, W.L. Johnson, Thermal stability and grain growth behavior of mechanically alloyed nanocrystalline Fe-Cu alloys, J. Appl. Phys. 73 (1993) 131-141.

[31] A.R. Kalidindi, C.A. Schuh, Phase transitions in stable nanocrystalline alloys, J. Mater. Res. 32 (2017) 1993-2002.

[32] R. Dannenberg, E.A. Stach, J.R. Groza, B.J. Dresser, In-situ TEM observations of abnormal grain growth, coarsening, and substrate de-wetting in nanocrystalline Ag thin films, Thin Solid Films 370 (2000) 54-62.

[33] R. Dannenberg, E. Stach, J.R. Groza, B.J. Dresser, TEM annealing study of normal grain growth in silver thin films, Thin Solid Films 379 (2000) 133-138.

[34] K.P. Almtoft, J. Bøttiger, J. Chevallier, N. Schell, R.M.S. Martins, Influence of the substrate bias on the size and thermal stability of grains in magnetron-sputtered nanocrystalline Ag films, J. Mater. Res. 20 (2005) 1071-1080.

[35] T. Kizuka, H. Ichinose, Y. Ishida, Atomic Structure and Thermal Stability of Nanocrystalline Silver, J. Jpn. I. Met. 55 (1991) 233-240.

[36] J. Xu, J.S. Yin, E. Ma, Nanocrystalline Ag formed by low-temperature high-energy mechanical attrition, Nanostruct. Mater. 8 (1997) 91-100.

[37] T. Goodrich, K. Bui, A. Athans, J. Cahalen, M. Osborne, P. Stokoe, Performance testing and evaluation of a Ag-W nano-crystalline silver alloy as a gold replacement in electrical connectors. In: 2014 IEEE 60th Holm Conference on Electrical Contacts (Holm), 2014, 1-7.

[38] F. Tang, D.S. Gianola, M.P. Moody, K.J. Hemker, J.M. Cairney, Observations of grain boundary impurities in nanocrystalline Al and their influence on microstructural stability and mechanical behavior, Acta Mater. 60 (2012) 1038-1047.

[39] T.Y. Huang, C.J. Marvel, P.R. Cantwell, M.P. Harmer, C.A. Schuh, Grain boundary segregation in Al–Mn electrodeposits prepared from ionic liquid, J. Mater. Sci. 51 (2016) 438-448.

[40] K. Babinsky, J. Weidow, W. Knabl, A. Lorich, H. Leitner, S. Primig, Atom probe study of grain boundary segregation in technically pure molybdenum, Mater. Charact. 87 (2014) 95-103.

[41] M.K Miller, A. Cerezo, M.G. Hetherington, Atom Probe Field Ion Microscopy, Clarendon Press, Oxford, 1996.

[42] A.J. Detor, M.K. Miller, C.A. Schuh, Solute distribution in nanocrystalline Ni–W alloys examined through atom probe tomography, Phil. Mag. 86 (2006) 4459-4475.

[43] K. Ishida, Effect of grain size on grain boundary segregation, J. Alloy. Compd. 235 (1996) 244-249.

[44] H.A. Murdoch, C.A. Schuh, Estimation of grain boundary segregation enthalpy and its role in stable nanocrystalline alloy design, J. Mater. Res. 28 (2013) 2154-2163.

[45] H. Bakker, Enthalpies in Alloys: Miedema's Semi-Empirical Model, Materials Science Foundations, Trans Tech Publications, Enfield, 1998.

[46] F.R. de Boer, Cohesion in Metals: Transition Metal Alloys, Elsevier, New York, 1998.

[47] L. Chen, J.L. Fan, H.R. Gong, Phase transition and mechanical properties of tungsten nanomaterials from molecular dynamic simulation, J. Nanopart. Res. 19 (2017) 118.

[48] C.N. Singman, Atomic volume and allotropy of the elements, J. Chem. Educ. 61 (1984) 137.

[49] K. Einarsdotter, B. Sadigh, G. Grimvall, V. Ozoliņš, V, Phonon instabilities in fcc and bcc tungsten, Phys. Rev. Lett. 79 (1997) 2073.

[50] D. McLean, Grain Boundaries in Metals, Clarendon Press, Oxford, 1957.

[51] S. Ruan, C.A. Schuh, Electrodeposited Al–Mn alloys with microcrystalline, nanocrystalline, amorphous and nano-quasicrystalline structures, Acta Mater. 57 (2009) 3810-3822.

[52] C.L. Liu, J.M. Cohen, J.B. Adams, A.F. Voter, EAM study of surface self-diffusion of single adatoms of fcc metals Ni, Cu, Al, Ag, Au, Pd, and Pt, Surf. Sci. 253 (1991) 334-344.

[53] P. Franke, D. Neuschütz, Thermodynamic Properties of Inorganic Materials, Springer, Berlin, Heidelberg, 2007.

[54] R. Kirchheim, On the solute-defect interaction in the framework of a defactant concept, Int. J. Mater. Res. 100 (2009) 483-487.

[55] T. Kresse, C. Borchers, R. Kirchheim, Vacancy–carbon complexes in bcc iron: correlation between carbon content, vacancy concentration and diffusion coefficient, Scr. Mater. 69 (2013) 690-693.

Figure Captions

Fig. 1. Schematics summarizing the instability mechanisms for nanocrystalline alloys which initially have solute segregation at grain boundaries. Scheme I: formation of second phases, such as intermetallic compounds and elemental clusters, which have the effect of depleting solute from the grain boundaries, increasing their energy and driving grain growth; scheme II: grain boundary migration away from the solutes; scheme III: solute dissolution off grain boundaries and into the bulk.

Fig. 2. Bright- and dark-field TEM images and SAED patterns of the nanocrystalline Ag-W alloys in the as-deposited state: (a) 0W, (b) 0.3W, (c) 1.3W, and (d) 1.9W.

Fig. 3. APT atom maps of Ag, W, and Ga of the nanocrystalline Ag-W alloys in the as-deposited state: (a) 0W, (b) 0.3W, (c) 1.3W, and (d) 1.9W. Ag, W, and Ga atoms are depicted by blue, red, and grey dots, respectively.

Fig. 4. Autocorrelation functions of W content for the nanocrystalline Ag-W alloys in the as-deposited state: (a) 0.3W, (b) 1.3W, and (c) 1.9W.

Fig. 5. 1D concentration profiles of the nanocrystalline Ag-W alloys in the as-deposited state: (a) 0.3W, (b) 1.3W, and (c) 1.9W. W and Ga profiles are depicted by red and grey lines, respectively, and W global content by APT is indicated by black dashed lines.

Fig. 6. Bright-field TEM images and SAED patterns of the nanocrystalline Ag-W alloys in the annealed conditions: (a) 0W, 100 °C, (b) 0.3W, 100 °C, (c) 1.3W, 100 °C, (d) 0W, 200 °C, (e)

0.3W, 200 °C, (f) 1.3W, 200 °C, (g) 0W, 300 °C, (h) 0.3W, 300 °C, (i) 1.3W, 300 °C, (j) 0W, 400 °C, (k) 0.3W, 400 °C, and (l) 1.3W, 400 °C.

Fig. 7. Average grain sizes of the 0W, 0.3W, and 1.3W alloys as a function of annealing temperature.

Fig. 8. Atom maps of Ga, W, and Ga+W of the nanocrystalline 1.3W alloy in the different annealed conditions: (a) 100 °C, (b) 200 °C, (c) 300 °C, and (d) 400 °C for 24 hours. Ga and W atoms are depicted by grey and red dots, respectively.

Fig. 9. 1D concentration profiles of the 1.3W specimen for different annealing temperatures: (a) 100 °C, (b) 200 °C, (c) 300 °C, and (d) 400 °C. W and Ga profiles are depicted by red and grey lines, respectively, and W global content by APT is indicated by black dashed lines.

Fig. 10. Comparison of grain-boundary segregation of W as calculated by the McLean isotherm of Eq. (3) with that determined by APT (after grain boundary thickness correction). The range of theoretical values reflects the range of segregation enthalpies supported by the Miedema model, while the range of the error bars on the experimental data reflect concentration ranges resulting from thickness corrections from t = 0.5 (higher concentrations) to 1.5 nm (lower concentrations).

Fig. 1

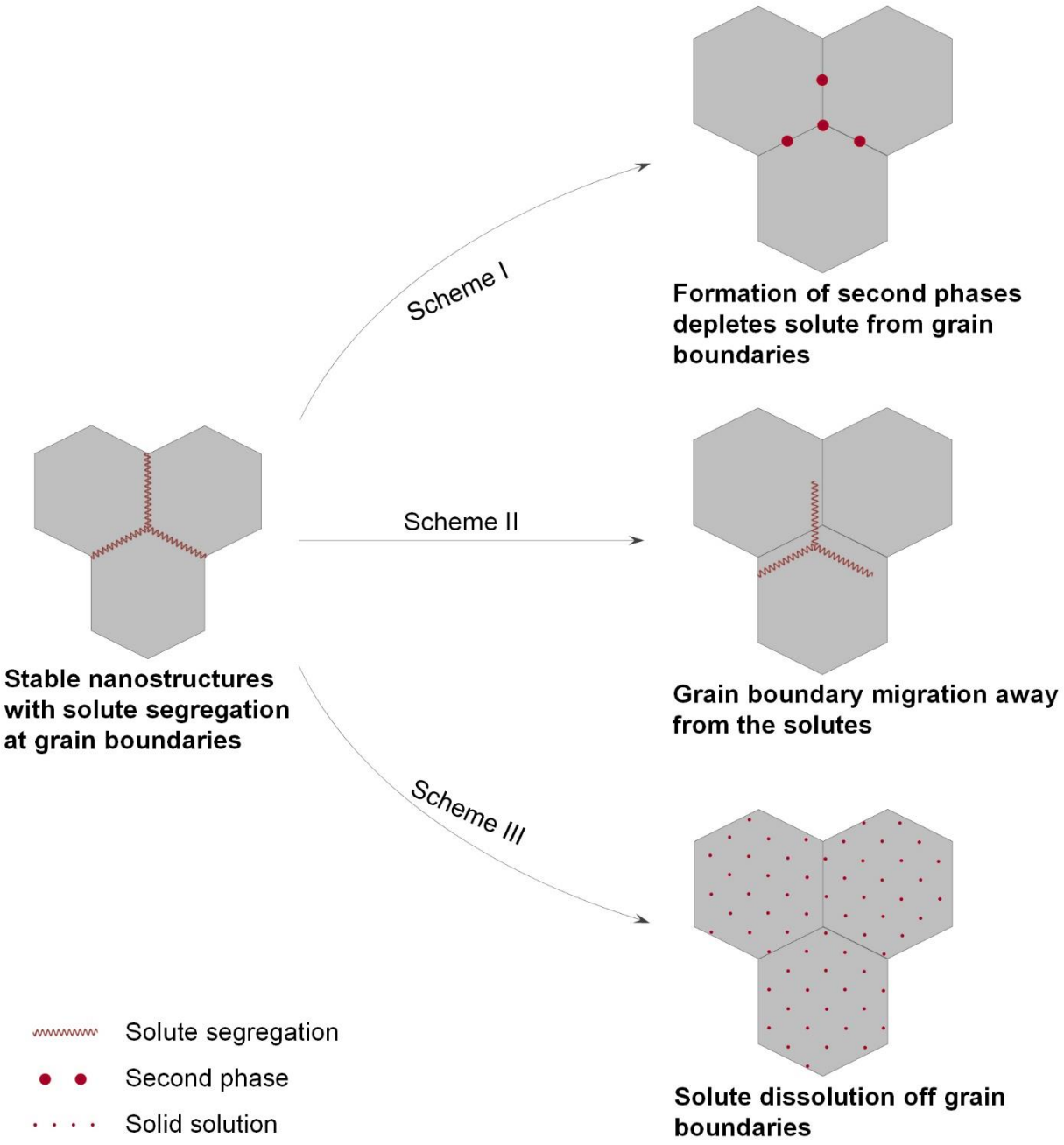
Scheme I
Formation of second phases depletes solute from grain boundaries
Scheme II
Stable nanostructures with solute segregation at grain boundaries
Grain boundary migration away from the solutes
Scheme III
Solute dissolution off grain boundaries
Solute segregation
Second phase
Solid solution

Fig. 2

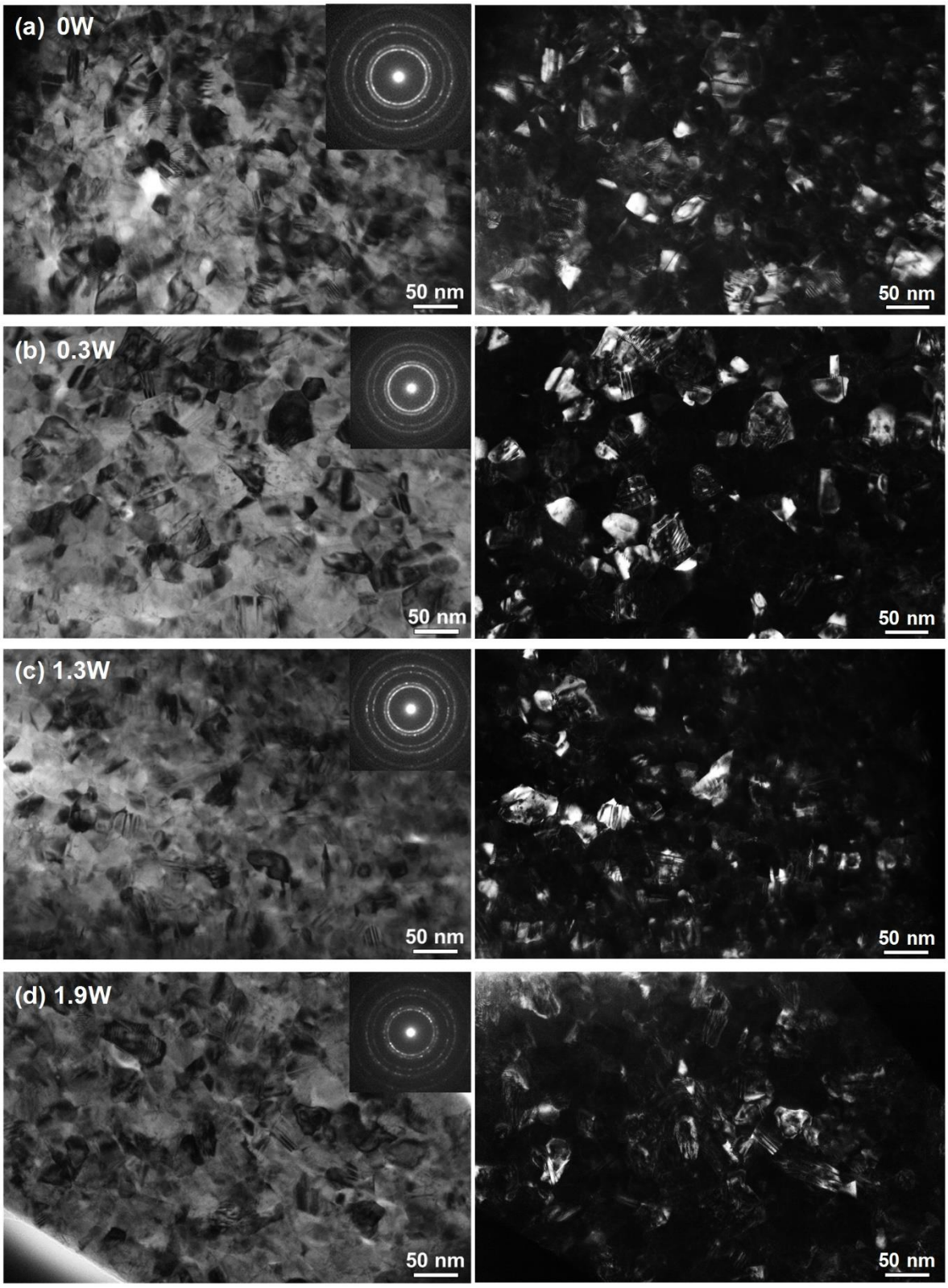

Fig. 3

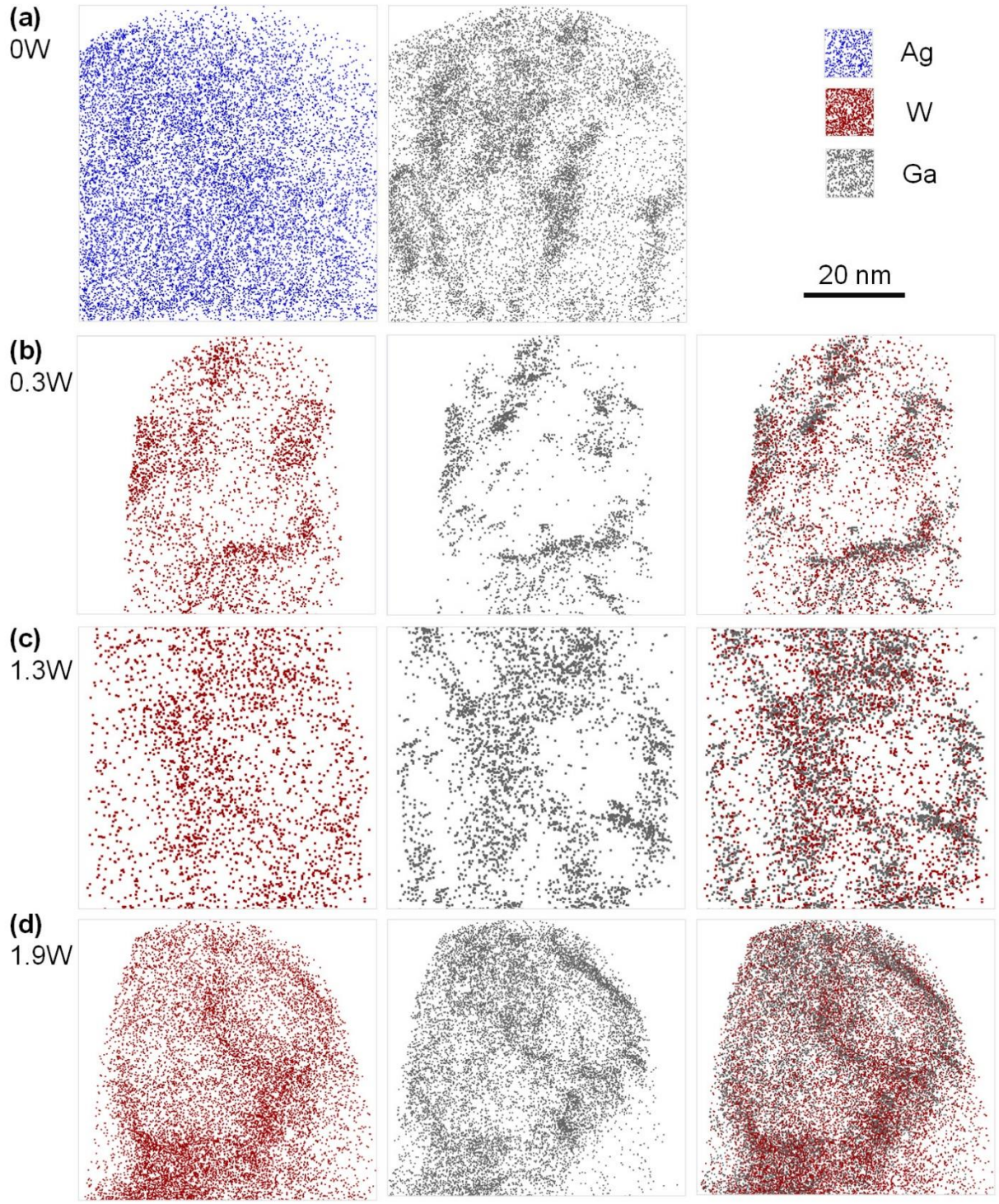

Fig. 4

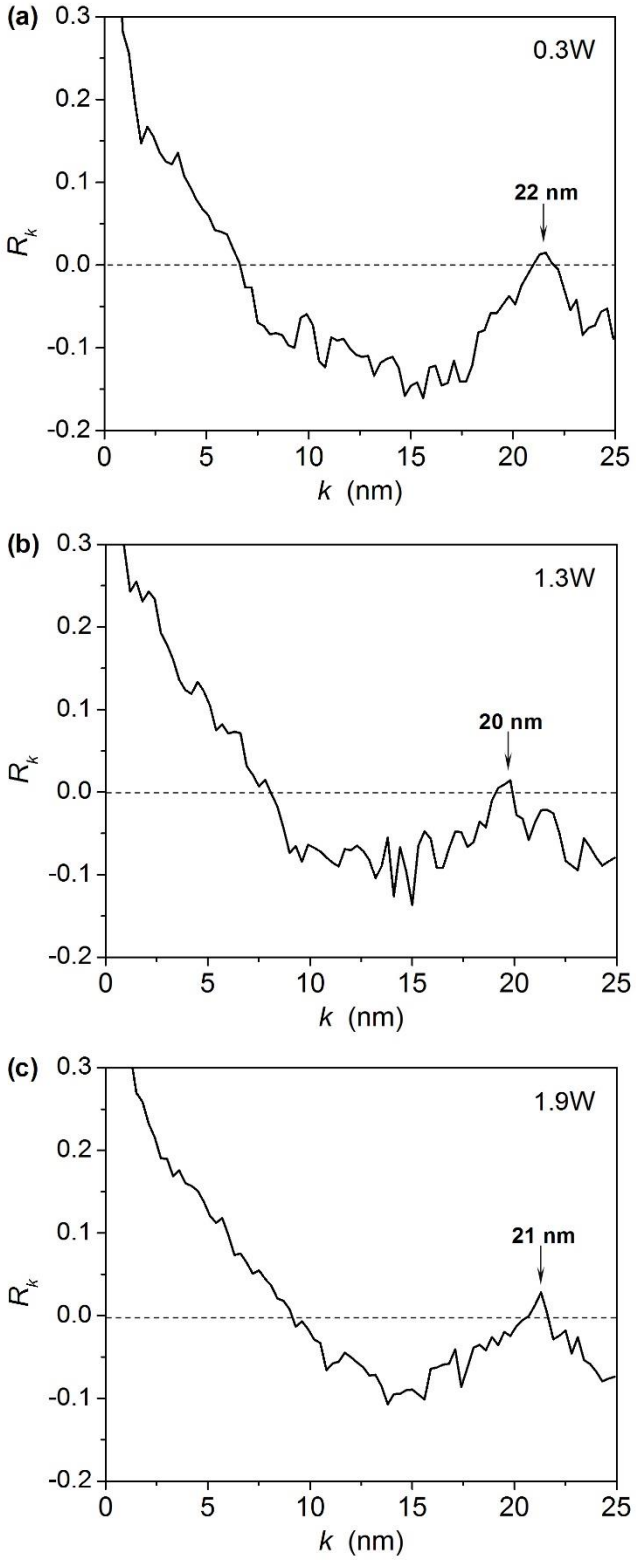
(a)
0.3W
22 nm
(b)
1.3W
20 nm
(c)
1.9W
21 nm
R_k
k (nm)
0.3
0.2
0.1
0.0
-0.1
-0.2
0
5
10
15
20
25

Fig. 5

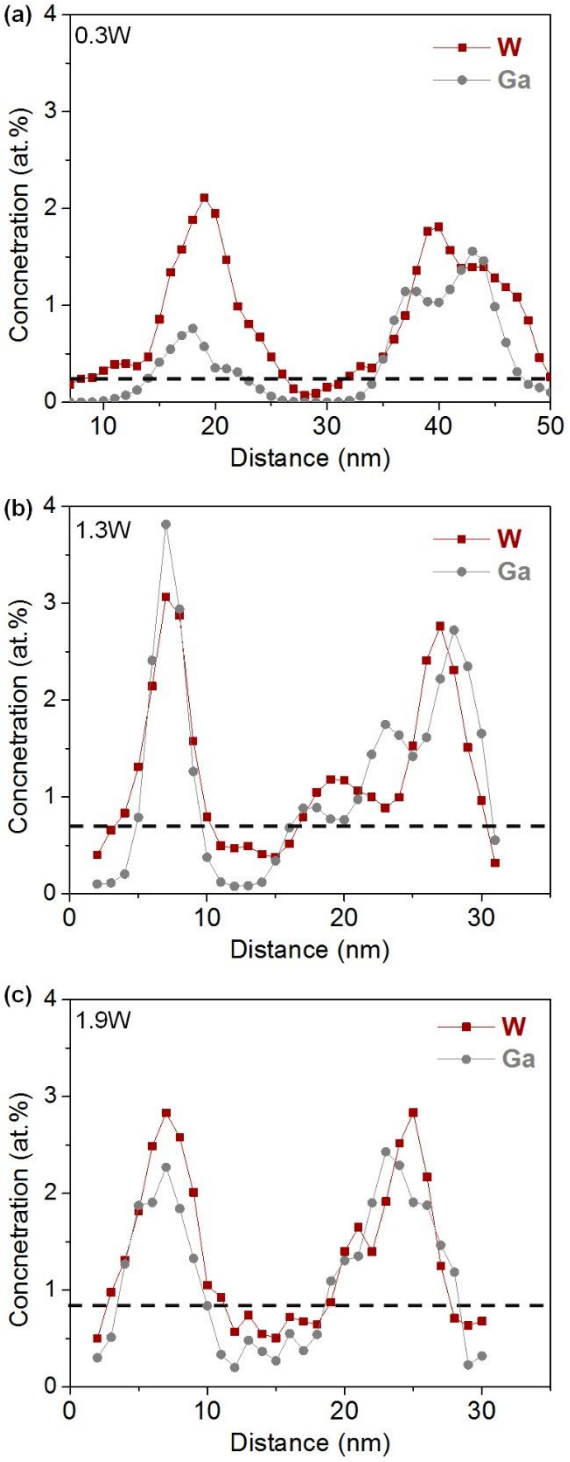
(a)
0.3W
W
Ga
Concnetration (at.%)
Distance (nm)
(b)
1.3W
W
Ga
Concnetration (at.%)
Distance (nm)
(c)
1.9W
W
Ga
Concnetration (at.%)
Distance (nm)

Fig. 6

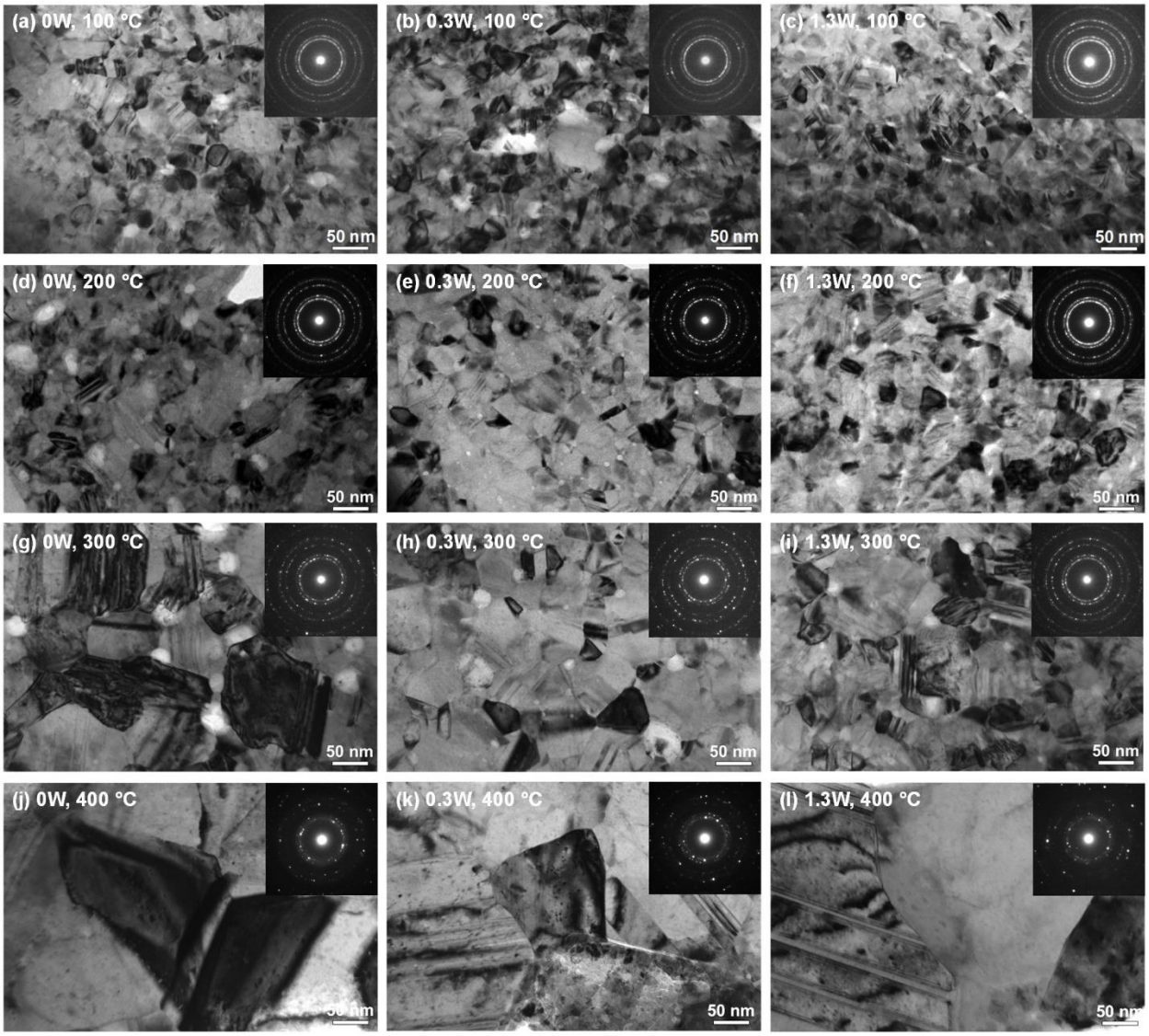
(a) 0W, 100 °C
50 nm
(b) 0.3W, 100 °C
50 nm
(c) 1.3W, 100 °C
50 nm
(d) 0W, 200 °C
50 nm
(e) 0.3W, 200 °C
50 nm
(f) 1.3W, 200 °C
50 nm
(g) 0W, 300 °C
50 nm
(h) 0.3W, 300 °C
50 nm
(i) 1.3W, 300 °C
50 nm
(j) 0W, 400 °C
(k) 0.3W, 400 °C
50 nm
(l) 1.3W, 400 °C
50 nm

Fig. 7

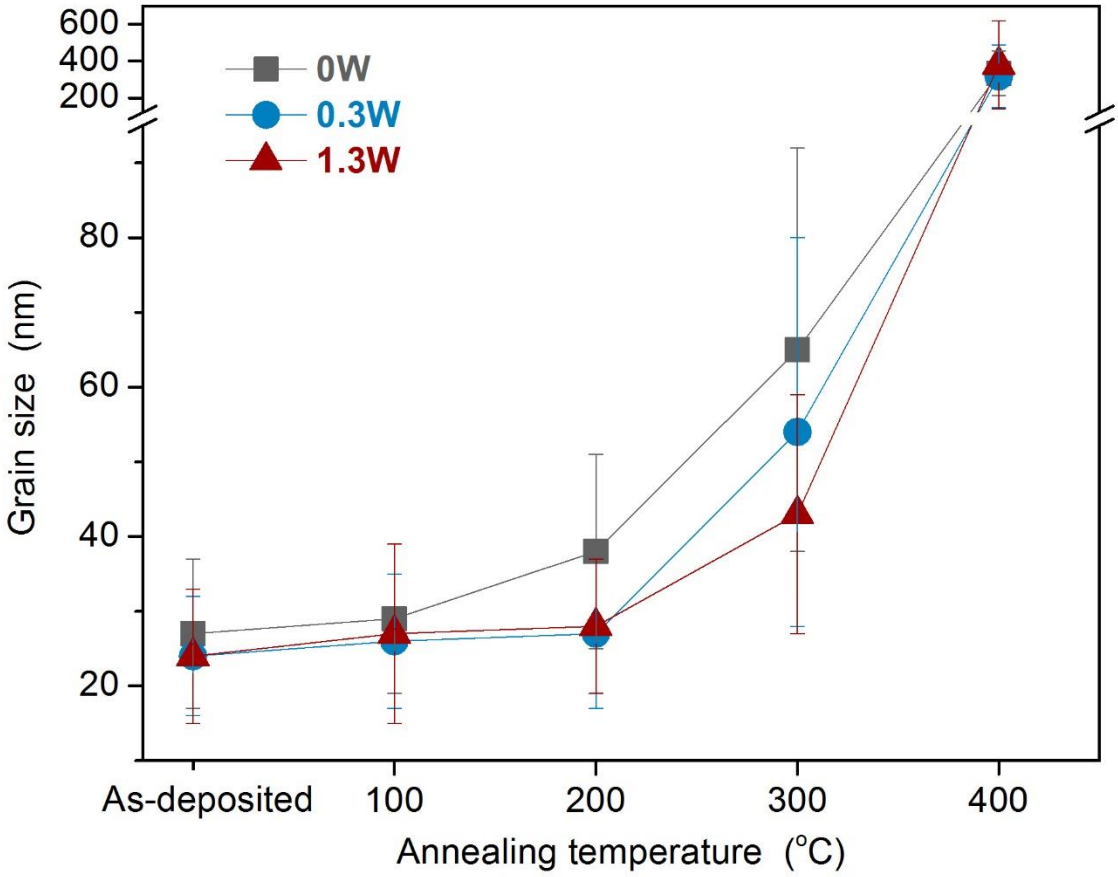
600
400
200
80
60
40
20
0W
0.3W
1.3W
Grain size (nm)
As-deposited
100
200
300
400
Annealing temperature (°C)

Fig. 8

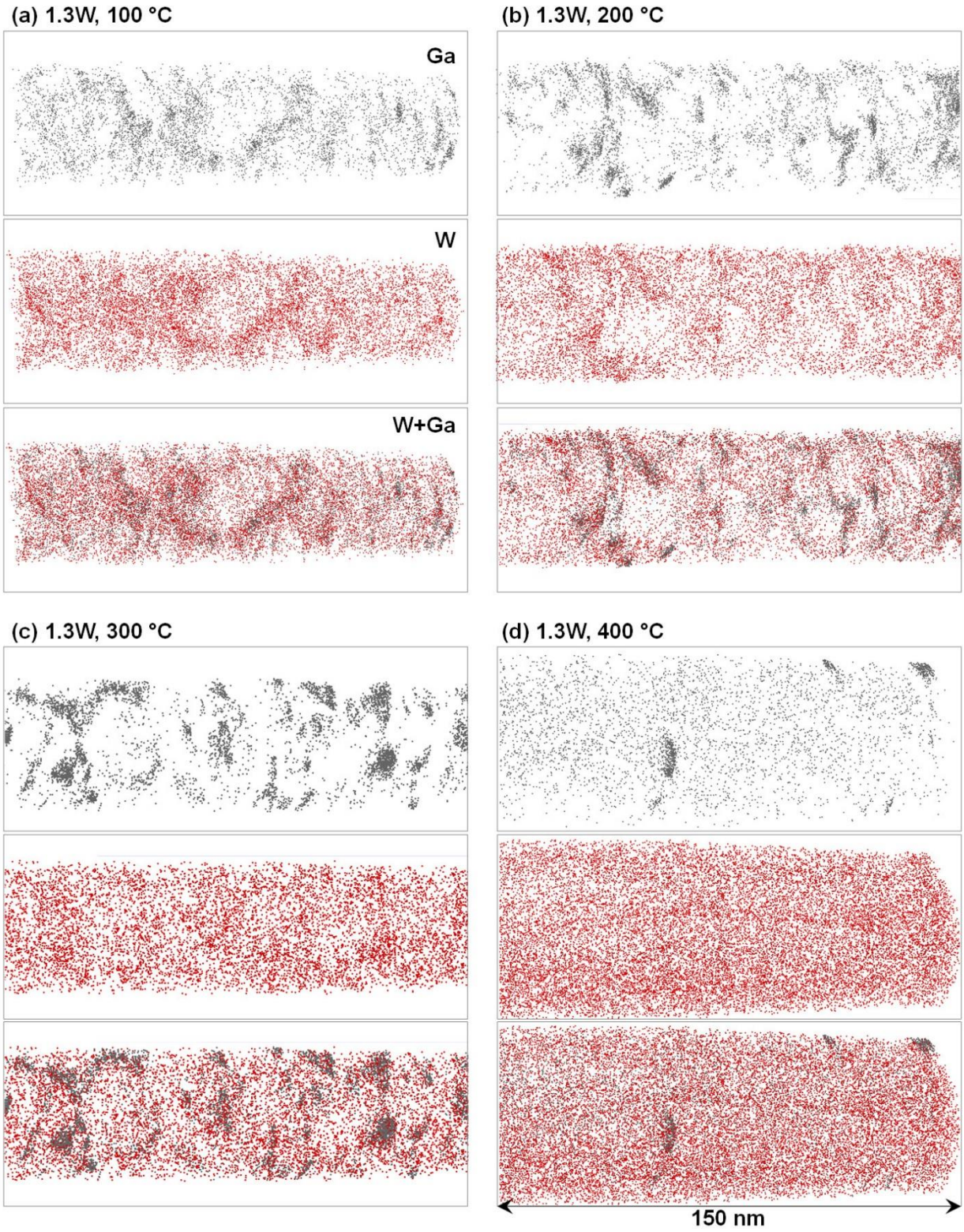

Fig. 9

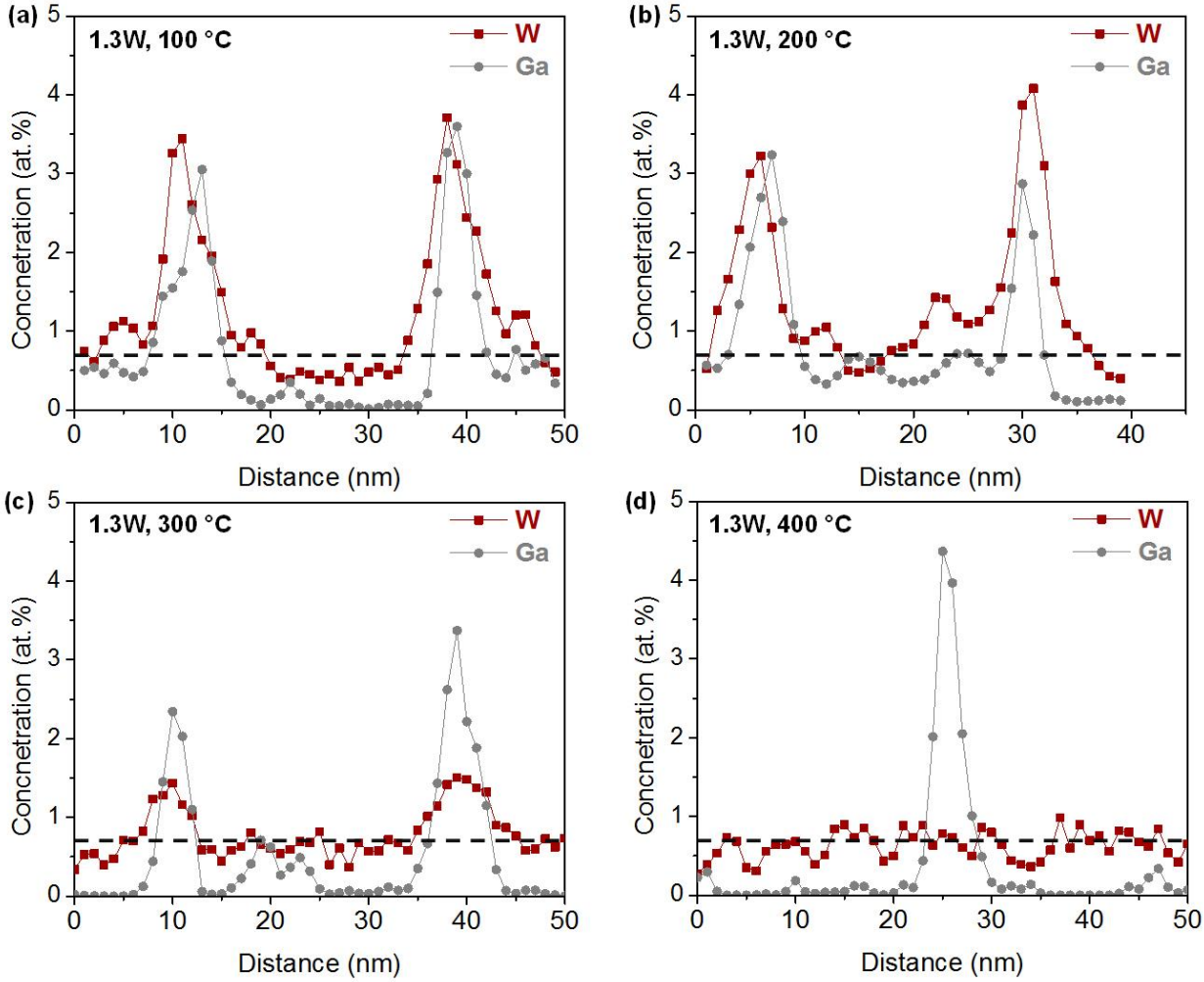
(a)
1.3W, 100 °C
W
Ga
Concnetration (at.%)
Distance (nm)
(b)
1.3W, 200 °C
W
Ga
Concnetration (at.%)
Distance (nm)
(c)
1.3W, 300 °C
W
Ga
Concnetration (at.%)
Distance (nm)
(d)
1.3W, 400 °C
W
Ga
Concnetration (at.%)
Distance (nm)

Fig. 10

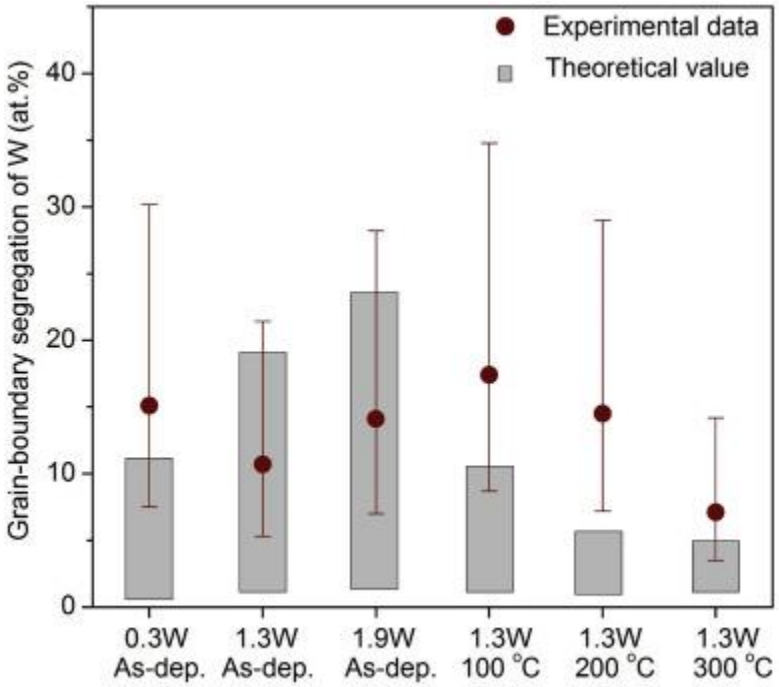
Experimental data
Theoretical value
Grain-boundary segregation of W (at.%)
0
10
20
30
40
0.3W As-dep.
1.3W As-dep.
1.9W As-dep.
1.3W 100 °C
1.3W 200 °C
1.3W 300 °C